Plasma ion assisted deposition of hafnium dioxide using argon and xenon as process gases

O. Stenzel,[1,*] S. Wilbrandt,[1] S. Yulin,[1] N. Kaiser,[1]
M. Held,[2] A. Tünnermann,[1,3] J. Biskupek,[4] and U. Kaiser[4]

[1]*Fraunhofer IOF, Albert-Einstein-Str.7, 07745 Jena, Germany*
[2]*Bte Bedampfungstechnik GmbH, Am Ganzacker 2, 56479 Elsoff, Germany*
[3]*FSU Jena, Institute of Applied Physics, Max Wien Platz 1, 07743 Jena, Germany*
[4]*Universität Ulm, Central Facility of Electron Microscopy, 89069 Ulm, Germany*
**olaf.stenzel@iof.fraunhofer.de*

Abstract: Hafnium dioxide films have been produced by plasma ion assisted electron beam evaporation, utilizing argon or xenon as working gases. The optical constants of the layers have been investigated by spectrophotometry, while X-ray reflection measurements (XRR), energy dispersive X-ray spectroscopy (EDX), and transmission electron microscopy (TEM) have been performed with selected samples. The correlation between structural and optical properties is discussed. With respect to optical quality, the application of xenon as working gas results in coatings with higher refractive index and smaller surface roughness than the application of argon. This effect is attributed to a more efficient momentum transfer from high energetic working gas ions or atoms to hafnium atoms during deposition.

©2011 Optical Society of America

OCIS codes: (160.4670) Optical materials; (310.3840) Materials and process characterization; (310.6860) Thin films, optical properties; (310.6870) Thin films, other properties; (310.1860) Deposition and fabrication.

References and links

1. W. T. Tang, Z. F. Ying, Z. G. Hu, W. W. Li, J. Sun, N. Xu, and J. D. Wu, "Synthesis and characterization of HfO_2 and ZrO_2 thin films deposited by plasma assisted reactive pulsed laser deposition at low temperature," Thin Solid Films **518**(19), 5442–5446 (2010).
2. J. M. Khoshman, A. Khan, and M. E. Kordesch, "Amorphous hafnium oxide thin films for antireflection optical coatings," Surf. Coat. Tech. **202**(11), 2500–2502 (2008).
3. R. Thielsch, A. Gatto, J. Heber, and N. Kaiser, "A comparative study of the UV optical and structural properties of SiO_2, Al_2O_3, and HfO_2 single layers deposited by reactive evaporation, ion-assisted deposition and plasma ion-assisted deposition," Thin Solid Films **410**(1-2), 86–93 (2002).
4. J. M. Khoshman and M. E. Kordesch, "Optical properties of a-HfO_2 thin films," Surf. Coat. Tech. **201**(6), 3530–3535 (2006).
5. T. Nishide, S. Honda, M. Matsuura, and M. Ide, "Surface, structural and optical properties of sol-gel derived HfO_2 films," Thin Solid Films **371**(1-2), 61–65 (2000).
6. N. Selvakumar, H. C. Barshilia, K. S. Rajam, and A. Biswas, "Structure, optical properties and thermal stability of pulsed sputter deposited high temperature HfO_x/Mo/HfO_2 solar selective absorbers," Sol. Energy Mater. Sol. Cells **94**(8), 1412–1420 (2010).
7. J. Capoulade, L. Gallais, J.-Y. Natoli, and M. Commandré, "Multiscale analysis of the laser-induced damage threshold in optical coatings," Appl. Opt. **47**(29), 5272–5280 (2008).
8. O. Stenzel, S. Wilbrandt, N. Kaiser, M. Vinnichenko, F. Munnik, A. Kolitsch, A. Chuvilin, U. Kaiser, J. Ebert, S. Jakobs, A. Kaless, S. Wüthrich, O. Treichel, B. Wunderlich, M. Bitzer, and M. Grössl, "The correlation between mechanical stress, thermal shift and refractive index in HfO_2, Nb_2O_5, Ta_2O_5 and SiO_2 layers and its relation to the layer porosity," Thin Solid Films **517**(21), 6058–6068 (2009).
9. O. Stenzel, S. Wilbrandt, M. Schürmann, N. Kaiser, H. Ehlers, M. Mende, D. Ristau, S. Bruns, M. Vergöhl, M. Stolze, M. Held, H. Niederwald, T. Koch, W. Riggers, P. Burdack, G. Mark, R. Schäfer, S. Mewes, M. Bischoff, M. Arntzen, F. Eisenkrämer, M. Lappschies, S. Jakobs, S. Koch, B. Baumgarten, and A. Tünnermann, "Mixed oxide coatings for optics," Appl. Opt. **50**(9), C69–C74 (2011).
10. B. Andre, L. Poupinet, and G. Ravel, "Evaporation and ion assisted deposition of HfO_2 coatings: Some key points for high power laser applications," J. Vac. Sci. Technol. **18**(5), 2372–2377 (2000).
11. D. Zhang, S. Fan, Y. Zhao, W. Gao, J. Shao, R. Fan, Y. Wang, and Z. Fan, "High laser-induced damage threshold HfO_2 films prepared by ion-assisted electron beam evaporation," Appl. Surf. Sci. **243**(1-4), 232–237 (2005).

#144260 - $15.00 USD Received 16 Mar 2011; revised 12 May 2011; accepted 18 May 2011; published 26 May 2011

12. M. Jerman, Z. Qiao, and D. Mergel, "Refractive index of thin films of SiO_2, ZrO_2, and HfO_2 as a function of the films' mass density," Appl. Opt. **44**(15), 3006–3012 (2005).
13. A. Kunz, A. Hallbauer, D. Huber, and H. K. Pulker, "Optische und mechanische Eigenschaften von RLVIP HfO_2-Schichten," Vak. Forsch. Praxis **18**(5), 12–16 (2006).
14. E. E. Hoppe, R. S. Sorbello, and C. R. Aita, "Near-edge optical absorption behavior of sputter deposited hafnium dioxide," J. Appl. Phys. **101**(12), 123534 (2007).
15. J. Aarik, H. Mändar, M. Kirm, and L. Pung, "Optical characterization of HfO_2 thin films grown by atomic layer deposition," Thin Solid Films **466**(1-2), 41–47 (2004).
16. M. Alvisi, F. De Tomasi, M. R. Perrone, M. L. Protopapa, A. Rizzo, F. Sarto, and S. Scaglione, "Laser damage dependence on structural and optical properties of ion-assisted HfO_2 thin films," Thin Solid Films **396**(1-2), 44–52 (2001).
17. A. Gatto, R. Thielsch, J. Heber, N. Kaiser, D. Ristau, S. Günster, J. Kohlhaas, M. Marsi, M. Trovò, R. Walker, D. Garzella, M. E. Couprie, P. Torchio, M. Alvisi, and C. Amra, "High-performance deep-ultraviolet optics for free-electron lasers," Appl. Opt. **41**(16), 3236–3241 (2002).
18. J. Bellum, D. Kletecka, P. Rambo, I. Smith, J. Schwarz, and B. Atherton, "Comparisons between laser damage and optical electric field behaviors for hafnia/silica antireflection coatings," Appl. Opt. **50**(9), C340–C348 (2011).
19. X. Cheng, Z. Shen, H. Jiao, J. Zhang, B. Ma, T. Ding, J. Lu, X. Wang, and Z. Wang, "Laser damage study of nodules in electron-beam-evaporated HfO_2/SiO_2 high reflectors," Appl. Opt. **50**(9), C357–C363 (2011).
20. Z. Jinlong, C. Xinbin, W. Zhanshan, J. Hongfei, and D. Tao, "HfO_2/SiO_2 chirped mirrors manufactured by electron beam evaporation," Appl. Opt. **50**(9), C388–C391 (2011).
21. S. Scaglione, F. Sarto, M. Alvisi, A. Rizzo, M. R. Perrone, and M. L. Protopapa, "Correlation between the structural and optical properties of ion-assisted hafnia thin films," Proc. SPIE **3902**, 194–203 (2000).
22. A. V. Tikhonravov, M. K. Trubetskov, T. V. Amotchkina, G. DeBell, V. Pervak, A. K. Sytchkova, M. L. Grilli, and D. Ristau, "Optical parameters of oxide films typically used in optical coating production," Appl. Opt. **50**(9), C75–C85 (2011).
23. G. Abromavicius, R. Buzelis, R. Drazdys, D. Perednis, and A. Skrebutenas, "Optimization of HfO_2, Al_2O_3 and SiO_2 deposition leading to advanced UV optical coatings with low extinction," Proc. SPIE **6596**, 65961N (2007).
24. P. Torchio, A. Gatto, M. Alvisi, G. Albrand, N. Kaiser, and C. Amra, "High-reflectivity HfO_2/SiO_2 ultraviolet mirrors," Appl. Opt. **41**(16), 3256–3261 (2002).
25. M. Gilo and N. Croitoru, "Study of HfO_2 films prepared by ion-assisted deposition using a gridless end-hall ion source," Thin Solid Films **350**(1-2), 203–208 (1999).
26. J. D. Targove and H. A. Macleod, "Verification of momentum transfer as the dominant densifying mechanism in ion-assisted deposition," Appl. Opt. **27**(18), 3779–3781 (1988).
27. O. Stenzel, S. Wilbrandt, K. Friedrich, and N. Kaiser, "Realistische Modellierung der NIR/VIS/UV-optischen Konstanten dünner optischer Schichten im Rahmen des Oszillatormodells," Vak. Forsch. Praxis **21**(5), 15–23 (2009).
28. M. Born and E. Wolf, *Principle of Optics* (Pergamon Press, 1968)
29. S. Wilbrandt, O. Stenzel, and N. Kaiser, "All-optical in-situ analysis of PIAD deposition processes," Proc. SPIE **7101**, 71010D (2008).
30. E. C. Freeman and W. Paul, "Optical constants of rf sputtered hydrogenated amorphous Si," Phys. Rev. B **20**(2), 716–728 (1979).
31. H. Finkenrath, "The Moss rule and the influence of doping on the optical dielectric constant of semiconductors—I," Infrared Phys. **28**(5), 327–332 (1988).
32. O. Stenzel, "A model for calculating the effect of nanosized pores on refractive index, thermal shift and mechanical stress in optical coatings," J. Phys. D **42**(5), 055312 (2009).

1. Introduction

Hafnium oxide is an important coating material today, and with respect to its optical properties it has several application fields. First of all, the combination of a refractive index in the region of 2.0…2.4 in the UV [1–3] with a bandgap around 5…5.8 eV [2,4–6] makes it a favorite high index UV material. In the past, therefore, many studies have been published that focus on the measurement and optimization of optical properties depending on the deposition technique [3,7–10]. With respect to deposition techniques applied, hafnium oxide appears as a quite versatile material: successful deposition has been reported for electron beam evaporation without (EBE) and with assistance (IAD and PIAD) [3,7,11,12], ion plating IP [7,8,13], magnetron sputtering MS [2,9,14], (dual) ion beam sputtering (D)IBS [7,9], pulsed laser deposition PLD [1], atomic layer deposition ALD [15] and sol gel coating [5].

Moreover, hafnium oxide is also an excellent candidate for a high index material in applications, where a high laser induced damage threshold (LIDT) of the coating is required [7,10,11,16,17]. More recent studies are therefore focused on LIDT measurement and optimization of multilayer stacks with hafnia as the high index coating [18,19]. In this regard,

#144260 - $15.00 USD Received 16 Mar 2011; revised 12 May 2011; accepted 18 May 2011; published 26 May 2011
(C) 2011 OSA

hafnium oxide is also in use in chirped mirrors for group velocity dispersion compensation in ultrashort laser pulse technology [20].

Many studies have shown, that hafnia layers may contain crystalline and amorphous fractions even if they have been deposited by (P)IAD [8,16,21].

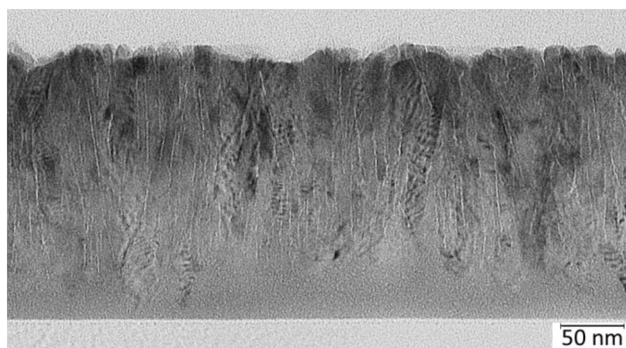

Fig. 1. TEM image of a 215 nm thick PIAD HfO_2-layer (120 V BIAS, rate 0.4 nm/s, deposition temperature 250°C, oxygen flow 15 sccm).

This is exemplified in Fig. 1, which presents the cross section transmission electron microscope (TEM) image of a single PIAD-deposited hafnia layer deposited at IOF in an earlier pre-study. After an initial amorphous growth phase, the layer is further polycrystalline. Tiny elongated pores appear between the crystalline grains (compare also some images in [8]).

Such a coating may appear optically inhomogeneous because the different phases can cause a refractive index gradient. Porosity is another possible reason for optical inhomogeneity. Refractive index gradients of hafnia layers deposited by different techniques have been quantified for example in [9] in the limits of Schröders approximation [22].

Figure 2 shows refractive indices n at a wavelength of 400 nm, depending on the deposition technique, as published in [1,4,7,13,23–25]. For MS and IBS, representative literature data corresponding to sufficiently dense coatings at a wavelength of 400 nm have not been identified in our literature study. We therefore decided to include further data into Fig. 2 which have been obtained by extrapolating 250 nm-values published in study [9] to the target wavelength of 400 nm; these data are shown as grey bars in Fig. 2 and seem us reasonable.

It is obvious that coatings deposited with some kind of energetic ion bombardment tend to exhibit higher refractive indices than conventionally evaporated samples. Highest refractive indices are usually achieved by IP, followed by PLD, IBS and MS. Samples prepared by EBE usually have the lowest indices, while IAD and PIAD are in-between the mentioned extreme cases.

The increase in refractive index is usually attributed to an increase in material density, caused as a result of momentum transfer from the accelerated noble gas ions or atoms to the atoms forming the layer [26]. The momentum transfer efficiency can be enhanced by suitable choice of a working gas. With respect to the mass number of hafnium atoms, xenon should be a better candidate for good momentum transfer process efficiency than argon, and indeed there are studies which have shown that the packing density of hafnia coatings can be enhanced when using xenon instead of argon as working gas [10,16]. In [16], the authors even report a clear increase in the refractive index at a wavelength of 250 nm with increasing momentum transfer parameter, obtained using IAD with a Kaufmann ion source. Nevertheless the highest reported refractive index of 2.25 (at a wavelength of 250 nm) in that study is not particularly high when comparing with more recent literature data, compare for example [9].

#144260 - $15.00 USD Received 16 Mar 2011; revised 12 May 2011; accepted 18 May 2011; published 26 May 2011
(C) 2011 OSA

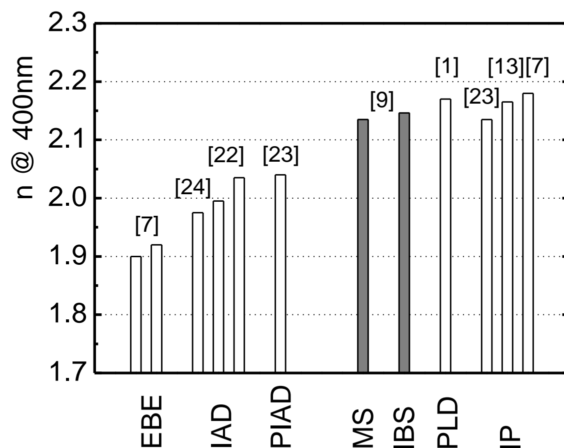

Fig. 2. Refractive index of hafnia coatings (literature data). References are indicated directly in the graph.

The focus of the present study is clearly on the PIAD technique. PIAD is a cost-efficient deposition technology that allows deposition of dense and stable coatings with high reproducibility. Therefore, it is commonly available nowadays in many industrial companies.

Nevertheless highest reported hafnia refractive indices stem from competing deposition techniques, such as IP or sputtering techniques (Fig. 2). In that connection it would be of great practical benefit to optimize PIAD deposition conditions with the goal to achieve refractive indices by PIAD which are comparable to best reported literature data.

The purpose of this study is therefore twofold: First of all we want to quantify the effects of a change in working gas in PIAD with an Advanced Plasma Source APS pro on refractive index, optical bandgap and surface roughness of hafnia layers. Secondly, it is our purpose to demonstrate that PIAD accomplished with xenon as working gas can result in hafnia coatings that come close by refractive index and surface roughness to high quality sputtered and ion plated samples.

2. Layer deposition

PIAD samples have been prepared in a Leybold Optics Syrus pro deposition system at IOF. During layer growth, additional energetic particle bombardment has been accomplished by means of the Leybold Optics Advanced Plasma Source APS pro. Main deposition parameters are summarized in Table 1.

The substrate temperature was around 110°C, and the oxygen flow was 15 sccm in all experiments. Thickness control has been accomplished by quartz monitoring.

Although according to Table 1 different deposition parameters are varied, the main goal of the investigation is nevertheless to highlight the differences in layers properties caused by application of either argon or xenon as the working gas during deposition. Therefore, as it follows from Table 1, every deposition experiment performed with xenon was accompanied by a reference experiment performed with argon, all other deposition parameters remaining the same. For quick recognition, xenon sample data are highlighted with a grey background in all tables.

In each run, one fused silica substrate (diameter 25 mm, thickness 1 mm) has been coated for optical measurements, as well as one both-side polished silicon shred for possible additional analytics (EDX or TEM). A further silicon wafer with diameter of 3 inch has been coated for mechanical stress measurements in selected charges only. In the last column in Table 1, the corresponding non-optical characterization methods as applied to the individual samples are listed. Selected samples have also been characterized by X-ray reflectometry XRR and X-ray diffraction XRD.

#144260 - $15.00 USD Received 16 Mar 2011; revised 12 May 2011; accepted 18 May 2011; published 26 May 2011
(C) 2011 OSA

Table 1. Main Deposition Parameters and Characterization Methods Used

No	BIAS V	Rate nm/s	Noble gas flow sccm	Non-optical analytics
1	100	0.2	12 Ar	
2			4 Xe	
3		0.3	12 Ar	XRR
4				EDX, stress
5				TEM, stress
6			4 Xe	XRR
7				EDX, stress
8				TEM, stress
9	110	0.2	12 Ar	
10			4 Xe	
11	120	0.2	12 Ar	XRR
12				stress
13			4 Xe	XRR
14				stress
15		0.3	12 Ar	XRR, XRD
16				EDX, stress
17				TEM, stress
18			4 Xe	XRR, XRD
19				EDX, stress
20				TEM, stress
21	130	0.2	12 Ar	EDX
22			4 Xe	EDX

In addition, hafnia films have been produced at bte Bedampfungstechnik GmbH, Germany, at high temperatures (350°C) without assistance. These films are produced by EBE with a deposition rate 0.5 nm/s and an initial oxygen flow of 65 sccm (with a fixed working pressure of $4.0*10^{-4}$ mbar). They are expected to be rather porous when compared to the samples produced by PIAD, and they only serve as further reference samples.

3. Layer characterization

3.1. Optical constants

Transmission and reflection spectra in the range of 200 –1000 nm were obtained by a Perkin Elmer Lambda 950 scanning spectrophotometer (equipped with a VN-measurement attachment [27]). From these spectra, film thickness as well as optical constants n (refractive index) and k (extinction coefficient) have been deduced from spectra fits in terms of a Lorentzian multioscillator model [28]. The relative accuracy in n- and d-determination is of the order of 1%.

3.2. Shift measurements

Some of the layers with lower refractive indices are likely to show a relevant thermal and vacuum shift because they are expected to be porous. For quantification purposes we have therefore measured the shift (more precisely a combination of thermal and vacuum shift) of these samples performing transmission measurements in the visible spectral range using the OptiMon process spectrophotometer [29].

These measurements have always been performed after more than one week of exposure to atmosphere, so that at least the large pores in the samples can be expected to be filled with water. First, a transmission measurement was performed in atmospheric conditions at room temperature. After that, the measurement chamber has been evacuated to high vacuum and heated up to a temperature of 100°C before making the second transmission measurement. From the differences in these spectra, the shift in optical thickness can be quantified as described elsewhere [8].

#144260 - $15.00 USD Received 16 Mar 2011; revised 12 May 2011; accepted 18 May 2011; published 26 May 2011
(C) 2011 OSA

3.3. Stress measurements

For stress measurements, the curvature of uncoated silicon wafers has been determined by a Tencor system. After deposition of the film the measurement of the curvature has been repeated, and from the difference in curvature, the layer stress has been calculated by Stoney's equation. In our convention, negative and positive stress values correspond to tensile and compressive stresses, respectively.

3.4. EDX

EDX measurements have been performed using a high resolution scanning electron microscope FE-SEM Sigma (Zeiss). The applied silicon drift detector Inca X-act (Oxford Instruments GmbH) is specified with a resolution of 129 eV. Spectra have been analyzed using INCA Software (INCA Energy 250).

3.5. TEM

Two xenon–assisted samples and their argon-assisted references deposited on silicon have been analysed by cross-sectional TEM analysis in order to evaluate the degree and specifics of their porosity as well as of their surface roughness. These measurements have been performed using a CM20 instrument (Philips, Netherlands) operating at 200 kV acceleration voltage. TEM samples were prepared by a standard routine via cutting, gluing, polishing, dimpling and Ar ion milling. Stepwise reduction of the Ar ion energy (from 5 kV to <1 kV) have been applied during the ion milling procedure to avoid possible modifications (amorphisation or layer intermixing) of the layered structure.

3.6. XRR and XRD

After deposition few selected samples were characterized with grazing incidence X-ray reflectivity (XRR) using a Bruker D5005 diffractometer operated with Cu-Kα radiation ($\lambda = 0.154$ nm) in symmetrical Θ-2Θ geometry. With some priority, we investigated samples where TEM images were available. Because the TEM cross sectional preparation of the samples is generally destructive, for XRR we had to use samples from other deposition runs prepared under identical conditions. The film thickness, material density and surface roughness were extracted from simulation of the reflective curves by the commercial program "WIN-REFSIM". Large-angle X-ray diffraction (XRD) of Cu-Kα radiation was applied to obtain information about the crystalline structure of the studied films (samples 15 and 18).

4. Results

4.1. Optical properties

Figure 3 shows UV-VIS transmission spectra of the pair of samples 17 (deposited with argon) and 20 (deposited with xenon). Immediately from these spectra it is obvious, that the application of xenon as working gas has led to a higher refractive index and to a shift of the absorption edge to longer wavelength, when comparing to the sample deposited with argon. For reference purposes, a sample deposited without assistance is also shown (in dash); it has a significantly lower refractive index, but higher UV transparency than the pair of assisted samples.

From transmission and reflection spectra, all assisted coatings appeared optically homogeneous. No refractive index gradients could be identified. Therefore, all transmission and reflection spectra have been fitted in terms of a homogeneous and isotropic layer model. Thus calculated thickness data as well as the refractive index values for the wavelength of 400 nm are given in Table 2. We also indicate an optical gap E_{04} defined here as the photon energy where the absorption coefficient $\alpha \equiv 4\pi k/\lambda$ equals 10000 cm^{-1} [30]. These data are listed in Table 2 together with results on the determined shift and layer stress. Regarding the choice of working gas, it turns out from Table 2 that the application of xenon instead of argon in all

#144260 - $15.00 USD Received 16 Mar 2011; revised 12 May 2011; accepted 18 May 2011; published 26 May 2011
(C) 2011 OSA

experiments has resulted in coatings with a higher refractive index (as measured on fused silica).

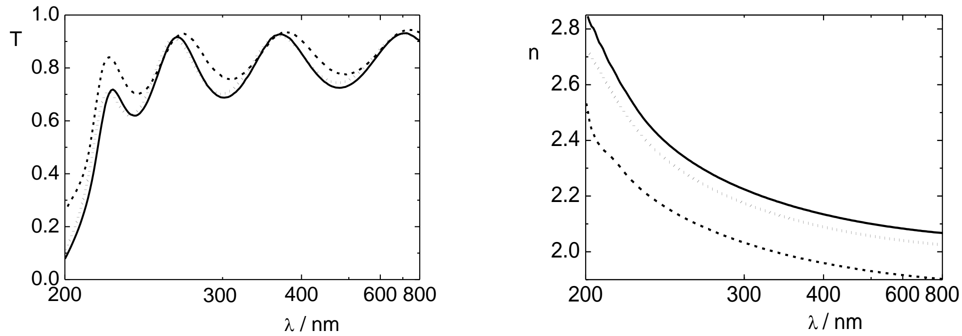

Fig. 3. On left: transmission spectra of sample 17 (deposited with argon, in dash) and sample 20 (deposited with xenon, solid line). A reference without assistance is shown as the dashed line.On right: corresponding refractive indices.

Table 2. Survey of Characterization Results[a]

Sample	n@ 400nm	d nm	E_{04} eV	Shift %	Mass density gcm^{-3}	RMS roughness nm	Stress MPa	Noble gas content at.%
Substr.	Fused silica				Silicon			
1	2.08	175	5.616	0				
2	2.122	170	5.575	0				
3	2.089	178	5.623	−0.5	9.29	1.4		
4	2.087	174	5.632	−0.4			−340	1.3
5	2.064	177	5.655	−1.38			−300	
6	2.102	173	5.581	−0.9	9.24	1.5		
7	2.134	172	5.581	0			n.d.	1.0
8	2.093	170	5.587	−0.33			−300	
9	2.053	179	5.642	0				
10	2.105	179	5.573	0				
11	2.053	188	5.648	0	9.1	1.1		
12	2.079	175	5.653	0			+ 215	
13	2.109	175	5.581	0	9.8	0.3		
14	2.109	173	5.618	0.11			+ 350	
15	2.091	176	5.618	0	9.36 9.4[*)]	1.4 1.2[*)]		
16	2.094	170	5.643	0			n.d.	2.8
17	2.089	173	5.633	−0.17			−340	
18	2.123	173	5.557	0	10.2 9.9[*)]	0.3 0.5[*)]		
19	2.133	172	5.578	0.06			+ 350	2.1
20	2.135	171	5.596	0			+ 345	
21	2.054	183	5.642	0				5.2
22	2.102	176	5.582	0				2.5

[a]n.d. means "not detectable."

[*)]second independent measurement, compare Table 3.

#144260 - $15.00 USD Received 16 Mar 2011; revised 12 May 2011; accepted 18 May 2011; published 26 May 2011
(C) 2011 OSA

Table 3. XRR Data Extracted for Samples 15 and 18 Deposited on Different Substrates

Sample	Substrate	RMS roughness nm	Mass density gcm^{-3}
15	Silicon	1.2 ± 0.1	9.4 + 0.1
	fused silica	1.6 ± 0.2	9.1 + 0.1
18	Silicon	0.5 ± 0.05	9.9 + 0.1
	fused silica	0.95 ± 0.1	9.4 + 0.1

The reference samples deposited without assistance are lower in refractive index, and show a weak but noticeable negative refractive index gradient. This can be a result of a depth-dependent degree of porosity. The porosity of the samples deposited without assistance is verified by the shift measurement, which resulted in rather strong shift values that scatter between -2.2% and -2.8%. At the same time, all non-assisted layers show tensile stress between −150 MPa and −230 MPa.

4.2. Structure-related results

According to Table 1, further structure-related investigations have been performed for selected samples deposited with plasma ion assistance.

Only a limited number of samples could be investigated by TEM. TEM measurements have been performed with samples deposited at a deposition rate of 0.3 nm/s. These samples showed highest refractive indices (Table 2) and are expected to have low noble gas content (see Sect. 4.3). Figure 4 shows transmission electron micrographs of the selected samples 5, 8, 17, and 20. The bright-field images on the left side verify the presence of pores in some of the coatings, while the porosity seems highest for sample 5 and decreases from top to bottom. Here the pores appear as the elongated bright structures arranged nearly perpendicular to the surface.

In sample 20, no pores could be detected. This is in good agreement to the result of shift measurements, which indicated strongest shift for sample 5, while sample 20 appeared shift free. Obviously, the pores are large enough to interchange water with the atmosphere.

On the right hand side of Fig. 4, the dark field images of the corresponding samples are shown. The bright regions in these graphs correspond to crystalline grains. From top to bottom, the crystallite size tends to decrease.

For samples 5, 8, and 17, the TEM bright-field images indicate on some surface roughness development. Corresponding information can also be obtained from the XRR measurements and is indicated in Table 2. For the samples deposited on Si-substrates with BIAS = 100 V, XRR indicates a significant rms surface roughness of about 1.5nm. The corresponding samples 5 and 8 appear rough in the TEM images, too. In the case of 120 V BIAS, we still obtain approximately the same roughness values for samples deposited with argon, while the surfaces of samples 13 and 18, deposited with xenon, are much smoother. This is also consistent with the results of the TEM investigations, when comparing the samples 17 and 20 (Fig. 4).

Regarding the choice of working gas, as a further trend it turns out from Table 2, that the application of xenon instead of argon results in coatings with a higher density (as measured on silicon).

In order to have an additional measure of crystallinity, the pair of sample 15 and 18 has been investigated by XRD. Because the TEM preparation of the utmost interesting samples 17 and 20 was destructive, we had to use samples from other deposition runs prepared under identical conditions. In this sense, sample 15 and 18 replaced the samples 17 and 20. To highlight the effect of the substrate, for these samples, XRR studies have been performed on silicon and fused silica substrates. The results are shown in Table 3.

The already mentioned increase in density caused by the transition from argon to xenon deposition gas is consistent with the data in Table 3, and is found on both substrates. Also, on both substrates, the xenon-assisted sample appears smoother than the corresponding argon-assisted reference sample. On the other hand, the HfO_2 - films deposited on silicon substrates

#144260 - $15.00 USD Received 16 Mar 2011; revised 12 May 2011; accepted 18 May 2011; published 26 May 2011
(C) 2011 OSA

are smoother and denser than the corresponding films deposited on fused silica. This result can be explained by the ion assistance effect which is more effective on a moderately conducting silicon substrate than on an insulating fused silica substrate due to substrate charging effects.

XRD measurements on these samples indicate the presence of HfO_2 crystallites with a size of approximately 4 nm (on both substrates). This result is in a qualitative agreement to the TEM results (first order of reflections of HfO_2 have been used to set up the dark-field illumination conditions) of the corresponding samples 17 and 20 (Fig. 4).

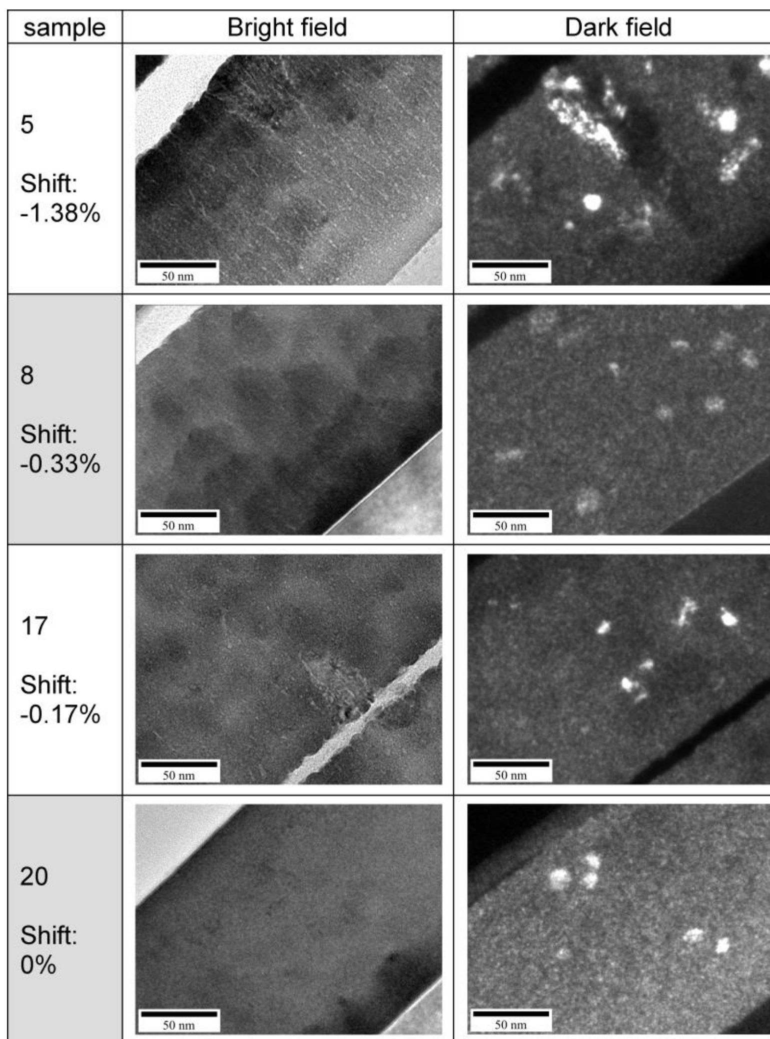

Fig. 4. Bright- (left) and dark- (right) TEM images of selected samples. On the right hand side the dark-field images of the corresponding bright-fields on the left hand side are shown. The bright spots in dark-field image indicate the size of crystalline grains. Note the decrease in crystallite size from top to bottom.

#144260 - $15.00 USD Received 16 Mar 2011; revised 12 May 2011; accepted 18 May 2011; published 26 May 2011
(C) 2011 OSA

4.3. Noble gas content

In order to determine the noble gas content in the studied films, three argon-assisted as well as three xenon-assisted samples have been studied by EDX. Again, priority was with samples prepared at a rate of 0.3 nm/s. In addition, the two 130 V BIAS samples (samples 21 and 22) have been included into the EDX study, because the low refractive index values obtained for these samples (Table 2) suggest a high noble gas content. The measured noble gas atom concentrations are given in Table 2. As a rule, the noble gas content inside HfO_2-filmes increases with BIAS voltage. This effect is shown in Fig. 5. It should however be noted, that the samples represented in Fig. 5 also differ in their growth rates. Keeping all other conditions fixed, a reduction in deposition rate should be also accompanied by an increase in noble gas content in the studied films. Therefore, the maximum argon content was really found in sample 21 deposited with maximum studied BIAS voltage (130 V) and minimum deposition rate (0.2 nm/s).

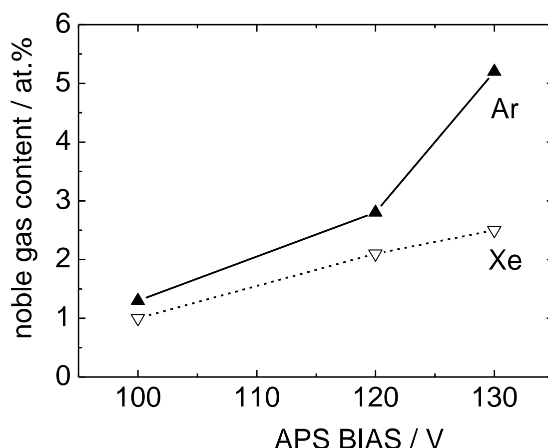

Fig. 5. Noble gas content in selected hafnia layers (Tables 1 and 2) versus BIAS voltage applied during deposition. Full triangles: argon assistance; Open triangles: xenon assistance. The straight connecting lines only serve as eye-guidelines.

5. Discussion

5.1 Optical properties

The main purpose of this study is to highlight the effect of xenon assistance during deposition process on the optical performance of PIAD-prepared hafnia coatings. For a direct comparison with argon assisted reference coatings, all refractive index and gap data from Table 2 are shown in Fig. 6 where the optical gap is plotted versus the refractive index at the wavelength of 400 nm.

Also, the figure shows data from reference samples deposited without any assistance.

It can immediately be recognized, that the assistance during deposition results in a significant increase in refractive index accompanied by a corresponding shrinkage in the optical gap. This is visualized by the dotted arrow. The three groups of data points (no assistance, argon assistance and xenon assistance) are well aligned along this arrow. It is moreover evident that principally all hafnia layers deposited with xenon assistance have higher refractive indices than the samples deposited with argon assistance. This confirms us that xenon assistance during deposition is more efficient than argon assistance. Together with the surface smothering effect reported in Sect. 4.2, the xenon assistance applied during the deposition process seems a prospective approach in development of enhanced high-index hafnia coatings with superior surface quality. In agreement with the Moss rule, however, high index coatings tend to have lower bandgap values than low-index samples [31]. In Fig. 6, this

#144260 - $15.00 USD Received 16 Mar 2011; revised 12 May 2011; accepted 18 May 2011; published 26 May 2011
(C) 2011 OSA

is reflected by the negative slope of the dotted arrow which indicates the effect of assistance. The practical conclusion is that the UV transparency is best for the non-assisted samples and lowest for the coatings deposited with xenon assistance (see also the measured UV extinction coefficient results in [10] in this regard).

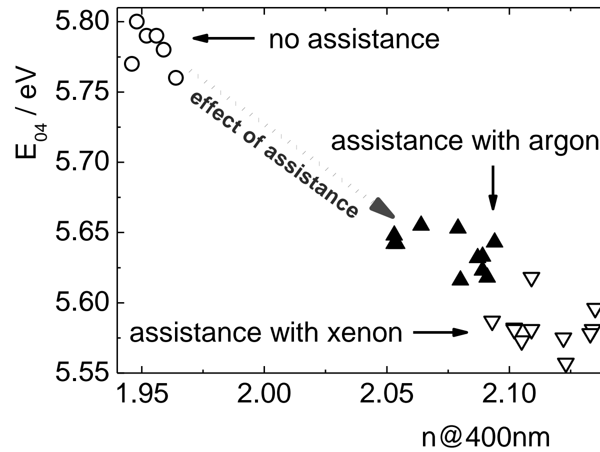

Fig. 6. Optical bandgap E_{04} vs. refractive index. Full triangles: argon assistance; Open triangles: xenon assistance; Open circles: no assistance.

When the optical bandgap (Fig. 7) and refractive index (Fig. 8) are plotted to the mass density (obtained from samples on silicon substrates), we recognize the expected trend of increasing refractive index and decreasing bandgap with increasing mass density. Moreover, the xenon-assisted samples tend to have higher densities than the argon assisted ones. The film densification achieved by xenon assistance can be attributed to a more efficient momentum transfer from the Xe ions or atoms to the hafnium atoms: The mass number of xenon (M = 131.3) is remarkably closer to that of hafnium (M = 178.5) than the mass number of argon (M = 40), which results in more efficient momentum transfer processes. The important role of efficient momentum transfer in deposition processes of high performance and dense optical coatings has already been reported in [26] with respect to fluoride coatings, and to hafnia in [10,16].

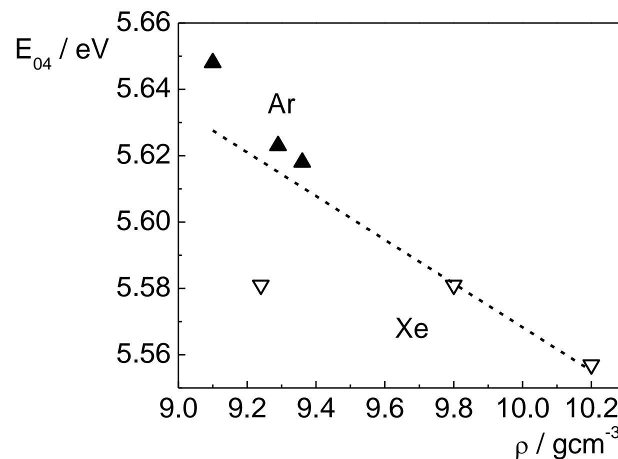

Fig. 7. Bandgap E_{04} vs. mass density. Full triangles: argon assistance; Open triangles: xenon assistance. The dashed straight lines indicate the result of a linear regression of the data.

#144260 - $15.00 USD Received 16 Mar 2011; revised 12 May 2011; accepted 18 May 2011; published 26 May 2011
(C) 2011 OSA

In an earlier study [8], refractive indices in the range between 2.03 and 2.08 at the wavelength of 400 nm were established for PIAD hafnia coatings deposited with conventional argon assistance. The data from Fig. 6 are in good agreement to these earlier investigations. In the same study, refractive indices of 2.174 and 2.197 extracted from different techniques have been reported for a hafnia coating produced by an ion plating technique, while the short scale surface roughness of this sample was around 1nm rms. When comparing these data with the findings from the present study, we can conclude that the xenon-assisted samples tend to exhibit optical properties intermediate between typical argon-assisted PIAD and ion plated samples, while the surface roughness values come close to the results achieved by ion plating. Of course, mechanical stress of the PIAD coatings remains much lower than that of ion plated samples.

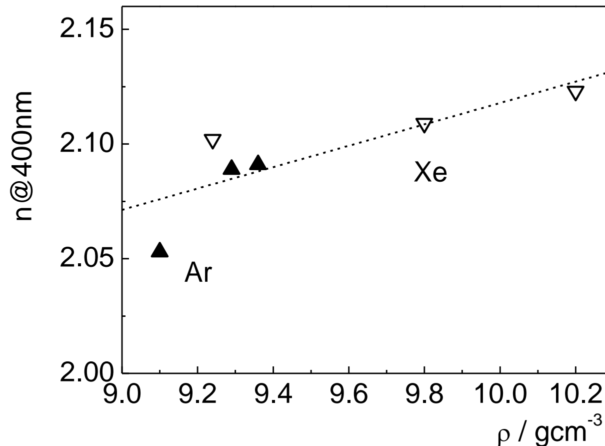

Fig. 8. Refractive index vs. mass density. Full triangles: argon assistance; Open triangles: xenon assistance. The dashed straight lines indicate the result of a linear regression of the data.

5.2. Structure-related properties

Although Figs. 7 and 8 seem to verify a clear correlation between optical properties and mass density, a shortcoming in our discussion is that optical data have been only obtained from samples deposited on fused silica, while structure-related data have been obtained only from selected samples deposited mainly on silicon substrates. There are nevertheless several attributes, which confirm us that correlations like shown in Figs. 7 and 8 really can be applied for all studied samples:

i. The results of shift measurements (performed on fused silica) are in excellent agreement with the indications on porosity as obtained from TEM investigations performed on silicon. Samples, which appear porous on silicon, exhibit a shift on fused silica. For that reason, in Fig. 4 the shift data have also been included (left column). Thus, the samples that appear shifting on silica must also be porous, and will consequently have a lower density than samples without shift. Exactly the same trend is observed when opposing shift data to density data obtained from XRR on silicon (Fig. 9). From Fig. 9 it is evident, that coatings with low density on silicon tend to exhibit shifts on fused silica. From these coincidences we conclude, that there is a monotonous correlation between the density measured on silicon and that relevant on fused silica.

ii. Of course, Fig. 9 also contains one point of low density, where no shift could be established. This point corresponds to the sample 11, deposited with argon assistance at low deposition rate. Once this study is focused on optical properties, we were unable to perform structure investigations with all samples. But the low deposition

#144260 - $15.00 USD Received 16 Mar 2011; revised 12 May 2011; accepted 18 May 2011; published 26 May 2011
(C) 2011 OSA

rate and the similarity of the properties of sample 11 to those of sample 21 suggest that sample 11 will also be rich in argon. High argon content, however, will have at least two consequences: It reduces the density of the coatings without causing any shift, and it impedes the accuracy in density determination by means of XRR. Therefore, to our opinion, the extraordinary behavior of sample 11 in Fig. 9 does not violate the validity of the general conclusions from point i).

iii. The comparative investigation of samples 15 and 18 on silicon and fused silica by XRR (Table 3) reveals the same trends in the evolution of density and surface roughness when changing the working gas on *both* types of substrates (compare the discussion in Sect. 4.2.). Moreover, no differences in crystalline structure of hafnia films deposited on different substrates could be observed by the XRD study.

iv. The relation between shift (measured on fused silica) and stress (measured on silicon) reveals the dependence typically observed for oxide coatings (Fig. 10) [8,32]. This also applies to the non-assisted samples, which are again included into this figure.

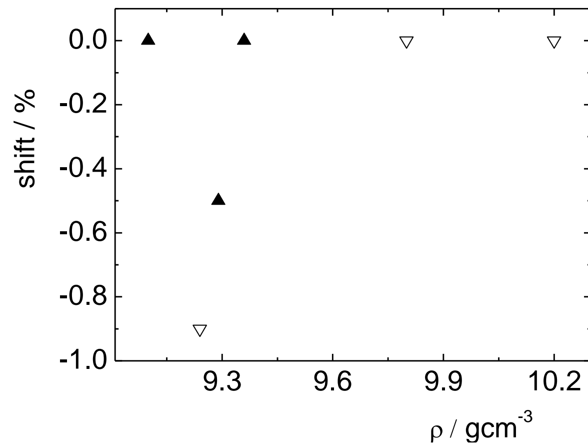

Fig. 9. Shift vs. mass density. Full triangles: argon assistance; Open triangles: xenon assistance.

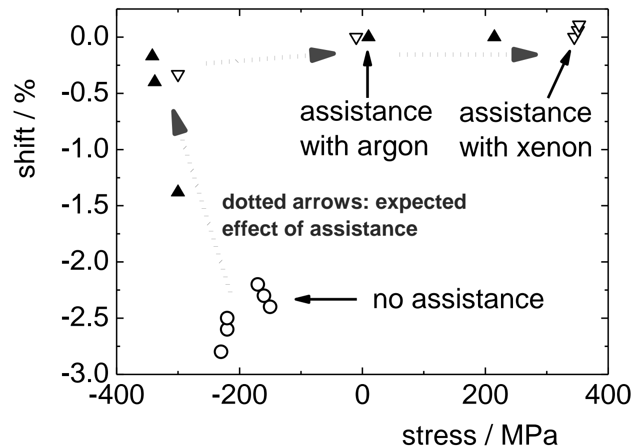

Fig. 10. Shift vs. mechanical stress. Full triangles: argon assistance; Open triangles: xenon assistance. Open circles: samples without assistance. The arrows only serve as eye-guidelines.

#144260 - $15.00 USD Received 16 Mar 2011; revised 12 May 2011; accepted 18 May 2011; published 26 May 2011
(C) 2011 OSA

In the frames of this study, we therefore conclude on a general agreement between the trends observed in structural parameters and optical properties. It was found that the discrepancies in hafnia densities for samples deposited on different substrates with Ar and Xe assistances are 0.3 g/cm^3 and 0.5 g/cm^3, respectively (Table 3). Once momentum transfer is more efficient for the xenon-assisted sample 18, it is understandable that the difference in densities on different substrates turns out to be higher for the xenon assisted samples. In Figs. 7 and 8, this discrepancy is expected to appear as a mere offset in abscissa scaling, but shall not have any crucial influence on the general type of correlation.

5.3. Comparison with literature data

In Fig. 11, roughness data presented in Table 3 are compared to literature data, taken from [7] (obtained there by means of AFM measurements). Roughness values published in [3] have not been included into Fig. 11 because of the significantly lower film thickness. Figure 11 thus only contains data points which stem from hafnia layers deposited on fused silica, while the film thickness is in the range between 170 nm and approximately 280 nm, as estimated for the 2H-layers at a wavelength of 1064 nm from [7].

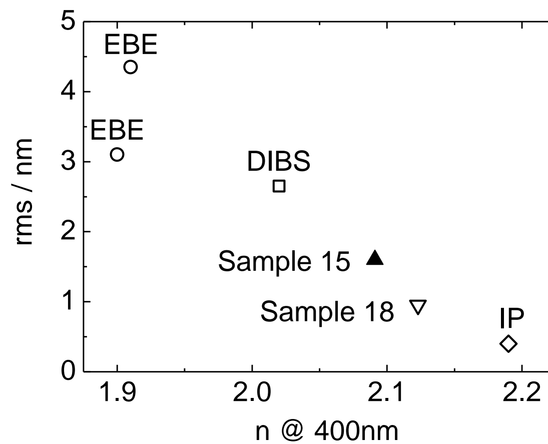

Fig. 11. rms-roughness vs. refractive index. Samples 15 and 18 originate from the present study. The other data are taken from [7]. DIBS denotes Dual Ion Beam Sputtering.

In Fig. 11, the roughness data are opposed to the refractive index at a wavelength of 400 nm. Two trends are obvious: Firstly, the roughness tends to decrease with increasing refractive index. This behavior can be attributed to the porosity of the films – a decrease in porosity gives rise to a higher refractive index and a smoother surface, in complete agreement to the trends visualized in Fig. 4. Secondly, the PIAD point corresponding to sample 18 (assistance with xenon) comes close to the literature value for the IP sample from [7].

In order to compare the refractive indices obtained in the frame of this study to literature data, we would like to return to the data presented in Fig. 2. In Fig. 12, these data are re-plotted together with highest refractive index values obtained in the present study. It is evident, that the xenon- assisted PIAD samples again come close to refractive indices that are usually achieved by sputtering or ion plating techniques. For direct comparison with other sources, we mention the corresponding refractive indices at a wavelength of 250 nm: it is 2.30 for the argon assisted sample, and 2.35 for the xenon assisted sample.

Hence, PIAD with xenon as working gas can result in hafnia coatings close by performance to high quality sputtered and IP samples.

#144260 - $15.00 USD Received 16 Mar 2011; revised 12 May 2011; accepted 18 May 2011; published 26 May 2011
(C) 2011 OSA

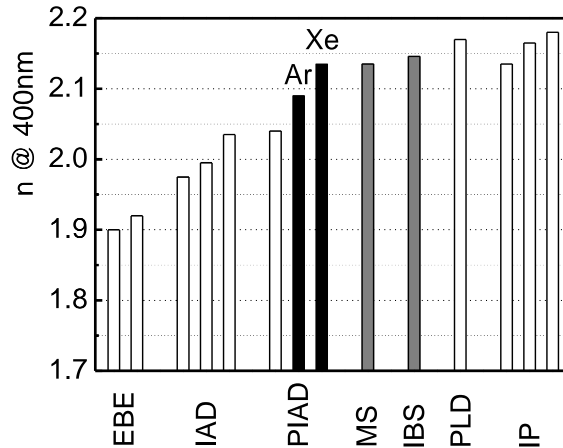

Fig. 12. refractive index of hafnia coatings: literature data from Fig. 2 and highest indices obtained in the present study (black bars).

6. Summary

We have presented experimental material on optical and structural properties of PIAD hafnia coatings. The main results of this study can be summarized as follows:

- PIAD of hafnium dioxide with xenon assistance results in higher refractive indices, lower band gaps and smoother film surfaces than PIAD with argon assistance.
- TEM and XRR data suggest a clear correlation between porosity, mass density, refractive index, shift and surface roughness of the layers.
- When comparing with literature data, xenon-assisted PIAD hafnia coatings come close to best values for refractive index and surface roughness published so far in the literature.

Future experiments will pursue deeper understanding of the film forming elementary processes determining energy- and momentum impact onto the substrate by detailed analysis of the plasma properties near the substrate during PIAD processes.

Acknowledgments

The authors of this article are grateful to Hanno Heisse (IOF) for sample preparation, Sebastian Haag (University of Applied Sciences Jena) for performing the literature study, to Sebastian Haag and Johannes Gäbler (University of Applied Sciences Jena) for assistance in manuscript preparation, and to Sabine Grözinger (Ulm University) for TEM sample preparation.

Many thanks are due to Nancy Bollwahn (IOF) for EDX measurements, Christina Hüttl (IOF) for XRR measurements, as well as Daniel Müller and Matthias Böhme (both from University of Applied Sciences Jena) for spectrophotometric measurements.

#144260 - $15.00 USD Received 16 Mar 2011; revised 12 May 2011; accepted 18 May 2011; published 26 May 2011
(C) 2011 OSA